Effects of Tube Length and Radius for Inner Surface Plasma Immersion Ion Implantation Using an Auxiliary Electrode

Dixon Tat-Kun Kwok, Xuchu Zeng, *Member, IEEE*, Qingchuan Chen, Paul K. Chu, *Member, IEEE*, and Terrence E. Sheridan

***Abstract*— Plasma immersion ion implantation of the inner surface of a finite-length small cylindrical tube with a coaxial, grounded auxiliary electrode is modeled using a two-dimensional particle-in-cell model. Various ratios of tube lengths against tube diameters are simulated. It is found that a peak in total accumulated dose is observed near the ends of the tube. Provided that it is long enough, the ions that come from the outside of the tube cannot pass through the middle-plane. That is, the tube can be divided conceptually into an "end" and a "middle" region, while the middle remains empty and all the flux goes to the end. In other words, a one-dimensional model can be applied to the "middle" region. The simulation results including the enhanced ion dose agrees with our experimental data.**

***Index Terms*—Inner surface, ion implantation, particle-in-cell, plasma application.**

I. Introduction

INNER surface modification of many industrial components, such as dies, bushings, pipes, etc. using plasma immersion ion implantation (PIII) is of practical importance and has attracted the attention of physicists and materials scientists [1]–[4]. One drawback of PIII of inner surfaces is low ion impact energy [5], [6]. It has been shown that by inserting a zero potential conductive auxiliary electrode along the axis of the implanted cylindrical tube, the average ion impact energy can be raised [7]. It has also been determined that the normalized auxiliary radius should range from 0.1–0.3 in order to maximize the dose and produce a larger number of ions with high impact energy [8].

In this article, we use a two-dimensional particle-in-cell (PIC) model [9] to investigate realistic cases in two dimensions, such as the important and practical situation when the cylindrical tube is of a finite length. The results acquired for different bore radii and tube lengths are reported. Our results reveal that the ions from outside of the tube are always implanted into a small region near the end thereby giving rise to nonuniform dose distribution along the interior surface. In a short tube, some of the ions pass through the midplane and arrive at the other end of the tube. However, if it is long enough, the ions from the outside of the bore cannot pass through the midplane. Hence, the tube can be divided conceptually into an "end" and a "middle" region, while the middle remains empty and all the flux goes to the end. In other words, simulation in the middle section can be simplified to be one-dimensional (1-D). The enhanced ion dose and other simulation results agree with our experimental data [10].

II. Kinetic Model and Numerical Simulation

Two basic assumptions are made for the ions. First, the condition is noncollisional. That is, the ion mean free path is greater than the sheath thickness, and it is valid in typical low pressure PIII applications. Second, the ions acquire directed motion only by the electric field. The electrons are assumed to be in thermal equilibrium, so that the electron density n_e is given by the Bolzmann's relationship

$$n_e = n_o \exp\left(\frac{e\phi}{kT_e}\right) \tag{1}$$

where n_o is the initial ion density, k is the Boltzmann's constant, and T_e is the electron temperature. Thus, we only need to follow the ion dynamics. Poisson's equation relates the potential ϕ to the electron density n_e and ion density n_i

$$\nabla^2\phi = -\frac{e}{\varepsilon_o}(n_i - n_e) \tag{2}$$

where ε_o is the permittivity in free space and e is the electron charge. The ions are governed by Newton's equations of motion [11]

$$\Delta\vec{r} = \vec{V}_a\Delta t - \frac{q}{2M}\nabla\phi(\Delta t)^2 \tag{3a}$$

$$\vec{V}_b = \vec{V}_a - \frac{q}{M}\nabla\phi\Delta t \tag{3b}$$

where q is the ion charge, M is the ion mass, $\vec{V}_a$ and $\vec{V}_b$ are the velocities before and after the time step Δt. The plasma quantities can be made dimensionless in cylindrical coordinates by normalization

$$\rho = \frac{r}{D}, \quad L = \frac{z}{D}, \quad T = t\omega_{pi}, \quad \Psi = \frac{\phi}{\phi_p}$$

$$N = \frac{n_i}{n_o}, \quad V^L = \frac{v_i^z}{v_{\max}}, \quad \text{and} \quad V^\rho = \frac{v_i^r}{v_{\max}}$$

Manuscript received June 4, 1998; revised October 6, 1998. This work was supported by City University of Hong Kong under Strategic Grant 7000730 and Hong Kong Research Grants Council Earmarked Grants 9040332 and 9040344.

D. T.-K. Kwok, X. Zeng, Q. Chen, and P. K. Chu are with the Department of Physics and Materials Science, City University of Hong Kong, Kowloon, Hong Kong (e-mail: paul.chu@cityu.edu.hk).

T. E. Sheridan is with the Plasma Research Laboratory, Australian National University, Canberra 0200, Australia.

Publisher Item Identifier S 0093-3813(99)02289-4.

where r and z are the radial and longitudinal distances, ϕ_p is the peak voltage of the pulse, v_i^r and v_i^z are the ion velocity components along the radial and longitudinal direction, $D = \sqrt{-4\varepsilon_o \phi_p / e n_o}$ is the ion-matrix overlap length, $\omega_{pi} = \sqrt{n_o e^2 \varepsilon_o M}$ is the ion plasma frequency, $v_{\max} = \sqrt{-2e\phi_p/M}$ is the velocity the ion would have if it fell through a potential drop ϕ_p, and M is the ion mass. For instance, $M = 28 \times 1.67264 \times 10^{-27}$ kg (nitrogen molecule, single positive charge), $n_o = 1 \times 10^9$ cm^{-3}, and $\phi_p = -50\,000$ V, we obtain $D = 10.5$ cm, $\omega_{pi} = 7.8679 \times 10^6$ s^{-1}, $T_{pi} = 1/\omega_{pi} = 0.127$ μs, and $v_{\max} = 5.8489 \times 10^7$ cm s^{-1}.

The vertical cross section of the cylindrical bore and auxiliary electrode is depicted in Fig. 1. The central gray bar symmetrically divides the tube into two equal halves. The midplane of the tube is another symmetry plane and only a quarter of the vertical cross section is thus required in our simulation. We assume that the top and right boundaries of the simulation regions are connected by a neutral plasma. Therefore, at these boundaries $\Psi = 0.0$. At the tube surface $\Psi = 1.0$ and on the surface of the auxiliary electrode $\Psi = 0.0$. At the bottom boundary $\partial\Psi/\partial L = 0.0$. The rise time of the applied voltage is set to zero and initially, and the ions are evenly distributed in the simulation region. We adopt the finite difference method to solve the equations [11]. After the position and velocity of each ion at a particle time step are derived, they will be weighted to the four corners of the mesh containing the ion. Provided the sheath is far away, the potential $\Psi \approx 0.0$ and the density of electron $n_e \approx n_o$ according to (1). The electrical acceleration will be weak and the heavy ions will not move at all. The densities of the electrons and ions will remain constant in the bulk plasma. When the ion hits the bore surface, it will be removed. The simulation model does not include the recombination process of the electrons and ions. We do not also include any generation mechanism of ion-electron pairs like secondary electron bombardment. The dose and impact angle surrounding the bombardment area will be automatically accumulated. If the ion crosses the bottom boundary, it is assumed that another ion from the other side with reverse longitudinal ion velocity will cross the boundary refilling the lost ion.

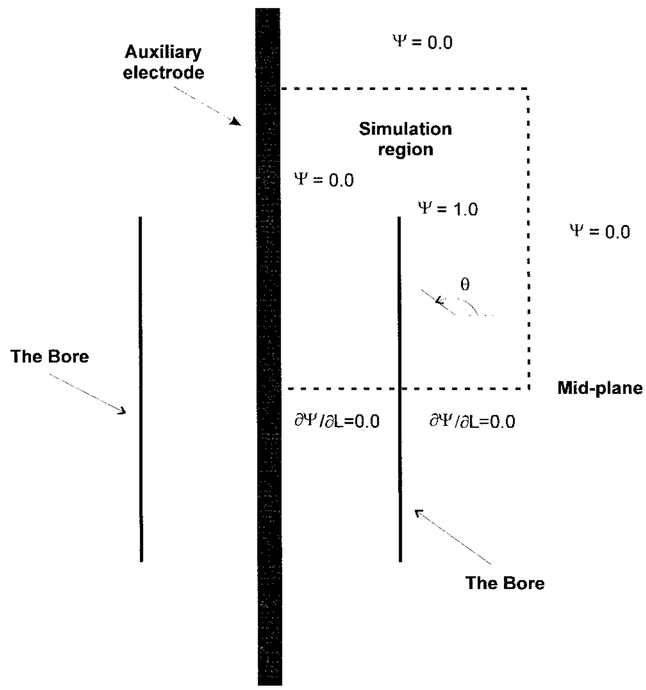

Fig. 1. Schematic diagram of the bore and auxiliary electrode defining the simulation region (demarcated by the dotted lines) and impact angle of the ion.

III. Results and Discussions

The auxiliary electrode radius is set to be equal to 0.1 D (in our case 1.05 cm), and the bore lengths and inner radii of the tube are varied. A total of four different cases are investigated: total tube length = 2 and 8 times D (half bore length = 1 and 4 times D, i.e., 10.5 and 42 cm) and inner radii = 0.5 (5.25 cm) and 1.0 D (10.5 cm). The thickness of the tube is zero. As shown in Fig. 1, a single grid line represents the tube. However, the electric field has different values inside the tube and outside of it. Thus, a double-valued electric field can be set inside and outside the tube even though the ion density is displayed as a single average value. We use zero rise time for the applied potential $|\phi_p| = 50$ kV and $T_e = 5$ eV. The other simulation parameters are: grid spacing $= 0.02D$ (0.21 cm) and time step $= 0.002T_{pi}$ (2.54×10^{-4} μs), where $T_{pi} = 1/\omega_{pi}$. The area of one cell $4.0 \times 10^{-4} D^2$, i.e., 0.0441 cm^{-2}. The maximum simulation area is $6 \times 3D^2$ and a total of 45 000 cells are considered. Each cell contains $1 \times 10^9 \times 0.0441 = 4.41 \times 10^7$ cm^{-1} nitrogen molecules. One hundred particles (ions) are initially uniformly placed in each cell. Therefore, each particle represents 4.41×10^5 cm^{-1} of nitrogen molecules in our example. The simulation lasted for $40T_{pi} = 5.08$ μs. We will continue the discussion of the result in a more general approach and not refer to any particular case. The normalized parameters are adopted.

A. Potential

The temporal evolution of the potential contour lines is displayed in Fig. 2 for $t = 2.0, 8.0, 20.0$, and $40.0T_{pi}$. The potential contour lines of bore radius equal to 1.0 D and bore length (half) equal to 1.0 and 4.0 D are depicted in Fig. 2(a) and (b). Fig. 2(c) and (d) illustrate the case when the bore radius is 0.5 D. Comparing Fig. 2(a) and (c) to Fig. 2(b) and 2(d), the potential contour lines pack more closely in the bore with inner radius = 0.5. The evolution of the potential sheath of the top region above 3.0(3.5) D of the long bore is identical to that of the short bore with bore radius equal to 1.0(0.5) D. In a deeper region of the long bore shown in Fig. 2(b) and (d), the potential sheath is vertical implying that there is only a radial electric field in this region.

B. Ion Density

The temporal evolution of the ion density is exhibited in Fig. 3. As shown in Fig. 3(a) and (b), the ions are bunched together near the inner surface of the tube (with radius = 1.0 D) at around 0.5 D from the top. However, when the tube radius is reduced to 0.5 D, the ion accumulation begins earlier and the location moves to around 0.15 D from the top

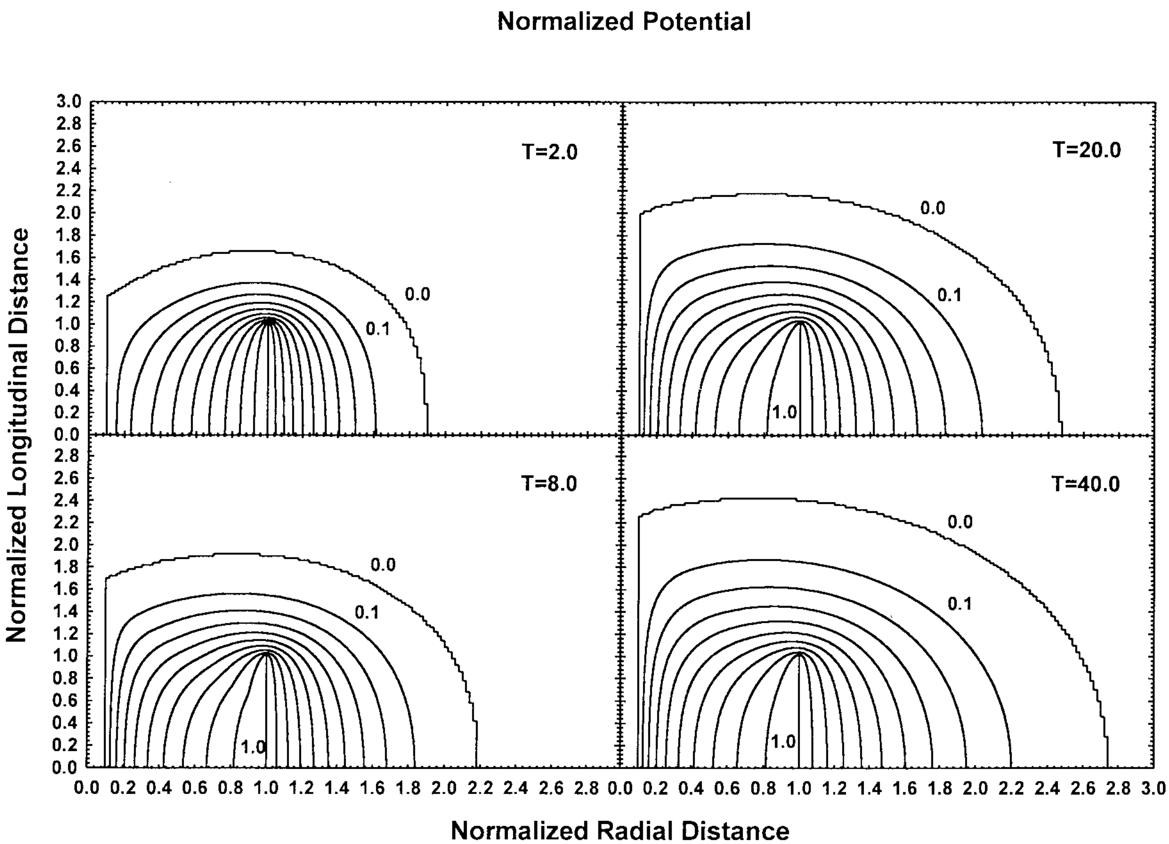

(a)

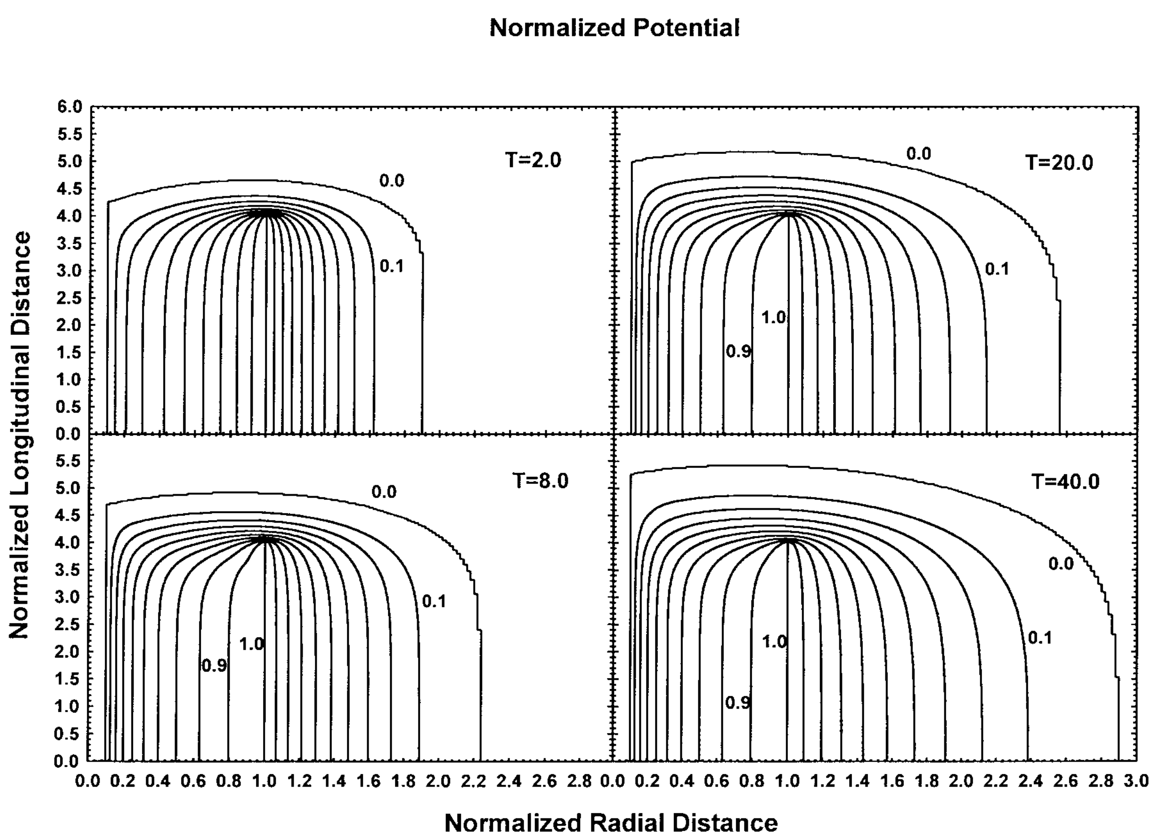

(b)

Fig. 2. Temporal evolution of the normalized potential for (a) radius = 1D, half-length = 1D and (b) radius = 1D, half-length = 4D.

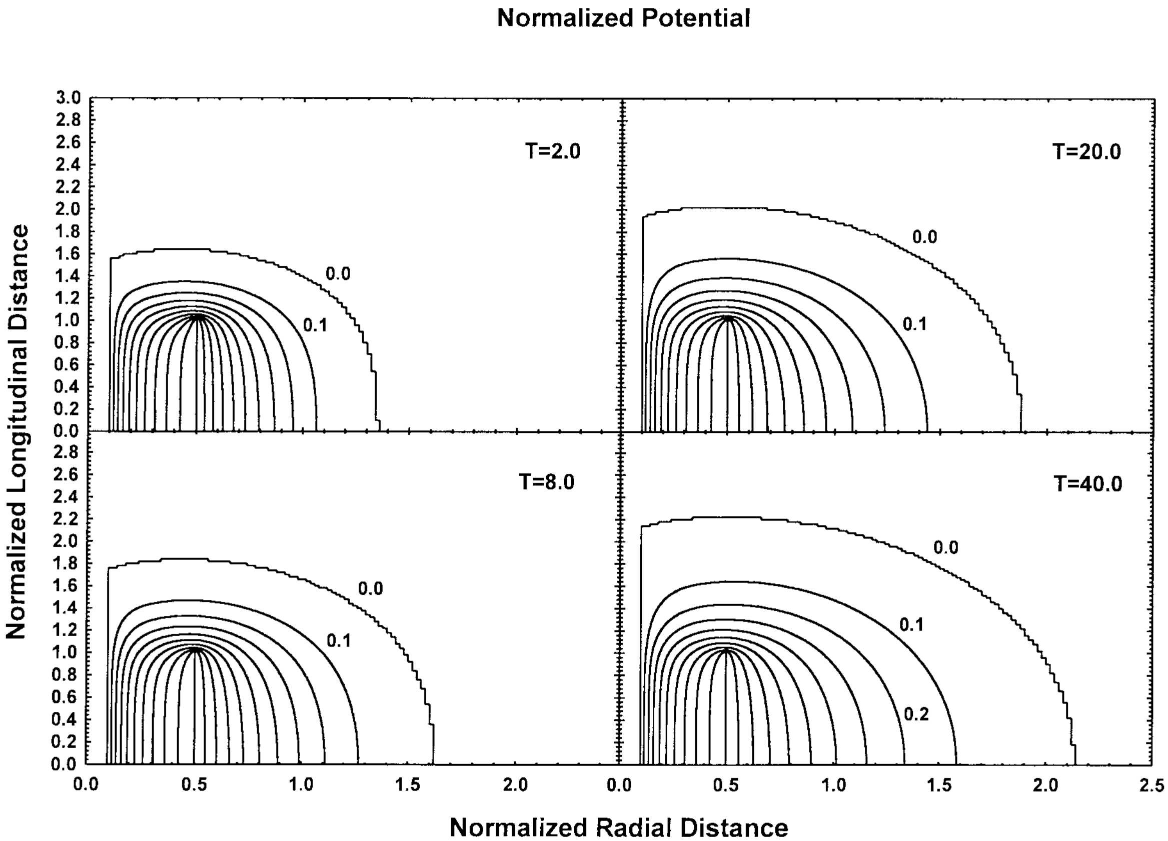

(c)

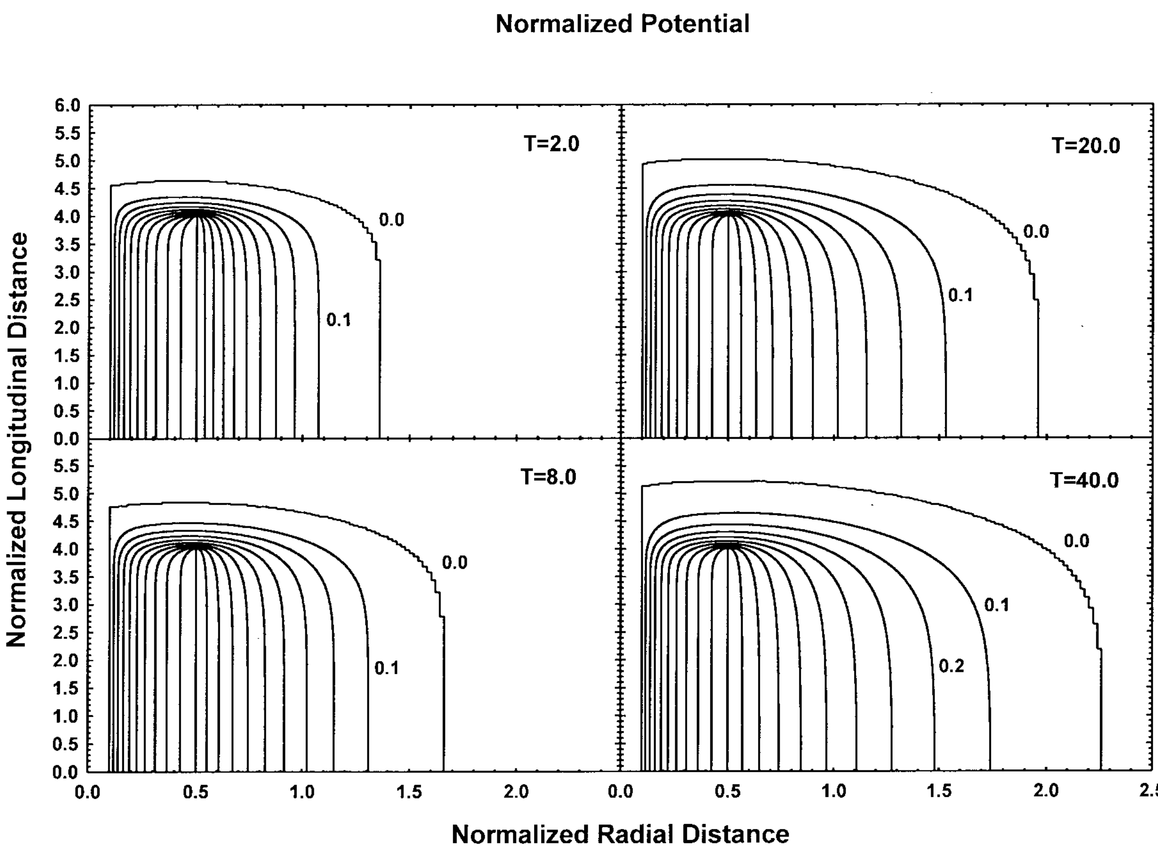

(d)

Fig. 2. *(Continued.)* Temporal evolution of the normalized potential for (c) radius = 0.5D, half-length = 1D and (d) radius = 0.5D, half-length = 4D.

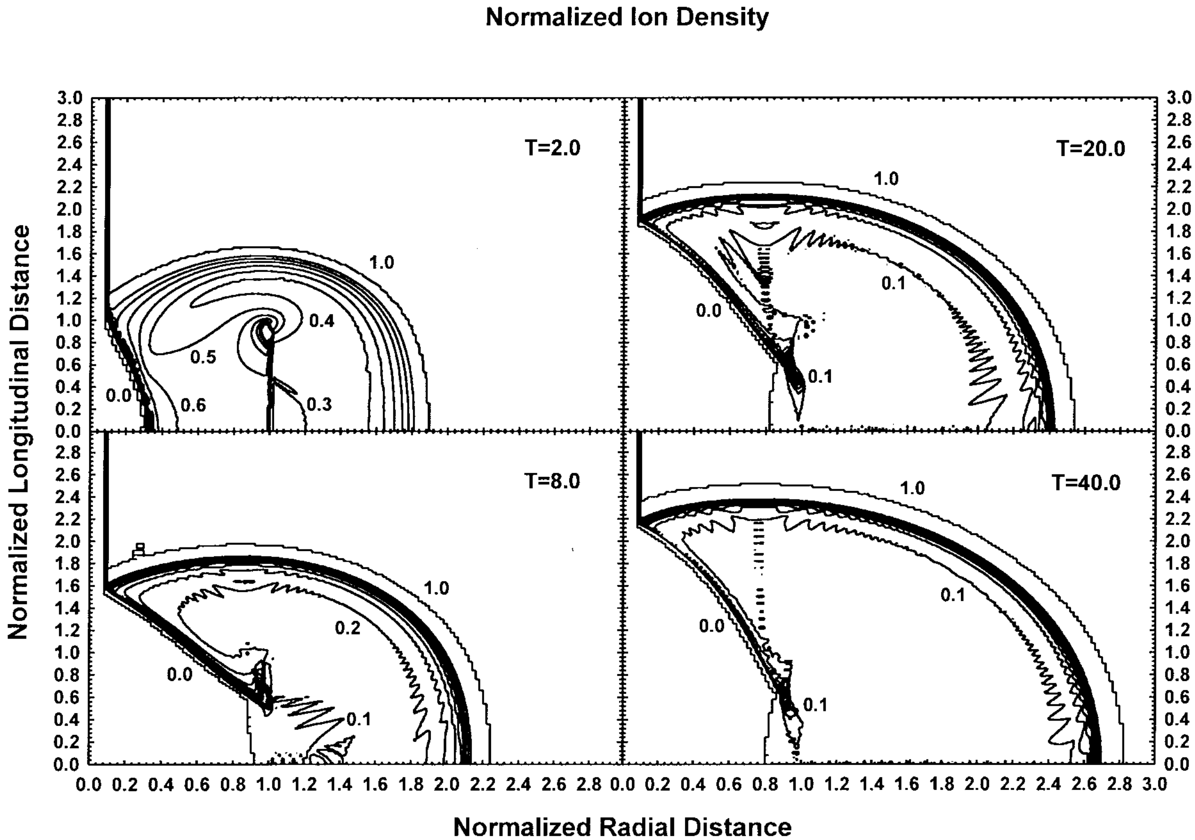

(a)

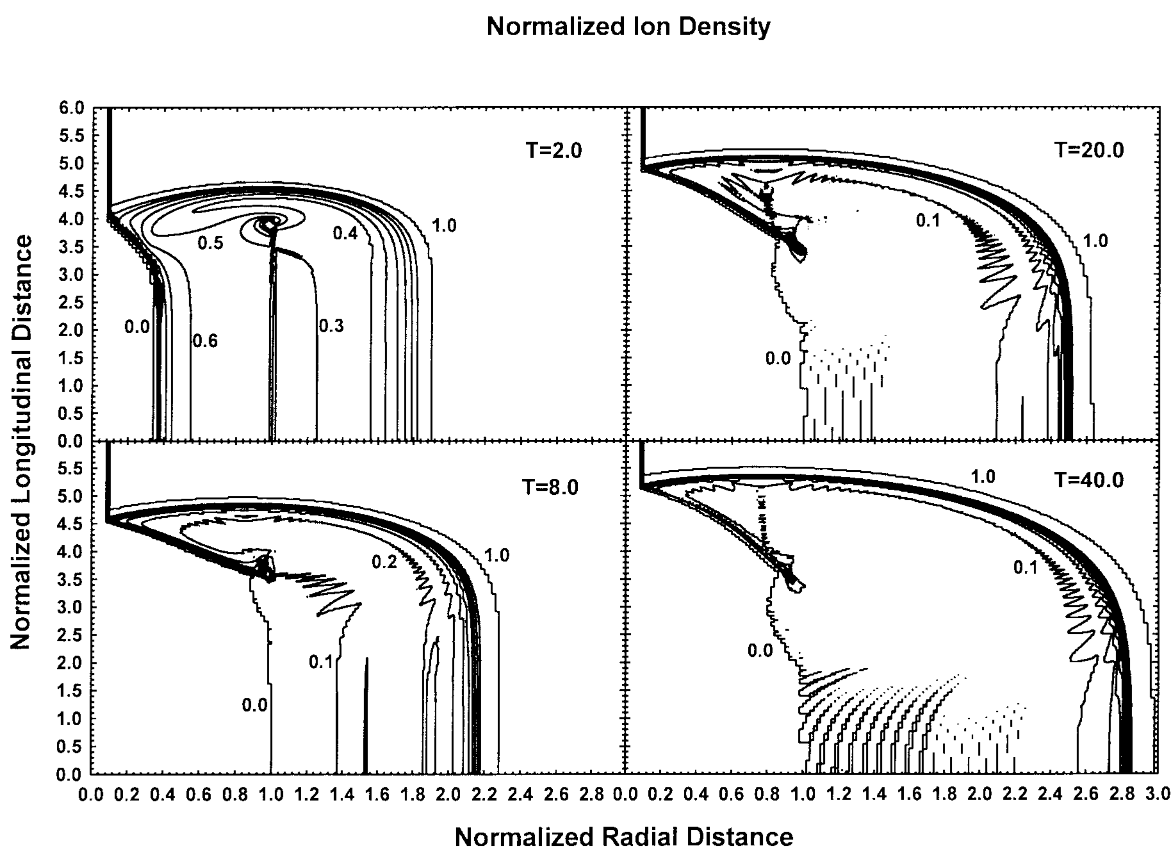

(b)

Fig. 3. Temporal evolution of the normalized ion density for (a) radius = 1D, half-length = 1D and (b) radius = 1D, half-length = 4D.

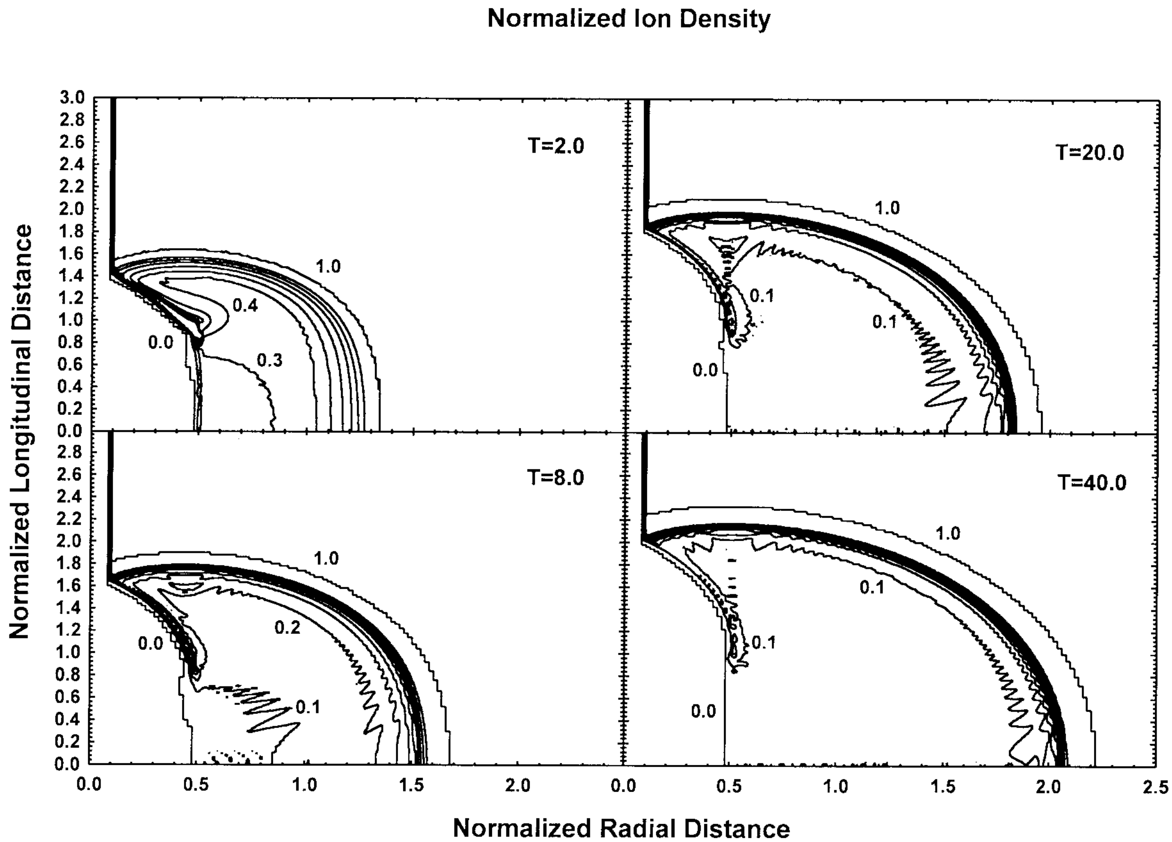

(c)

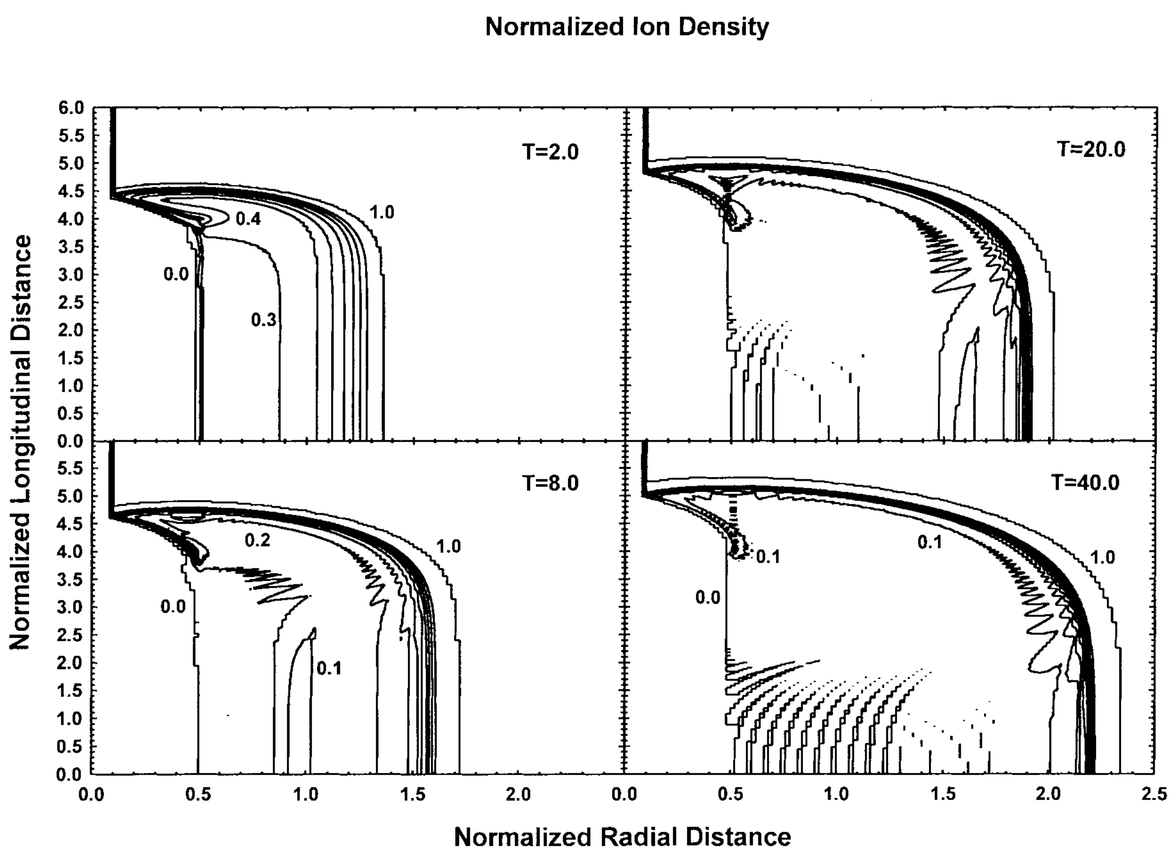

(d)

Fig. 3. *(Continued.)* Temporal evolution of the normalized ion density for (c) radius = 0.5D, half-length = 1D and (d) radius = 0.5D, half-length = 4D.

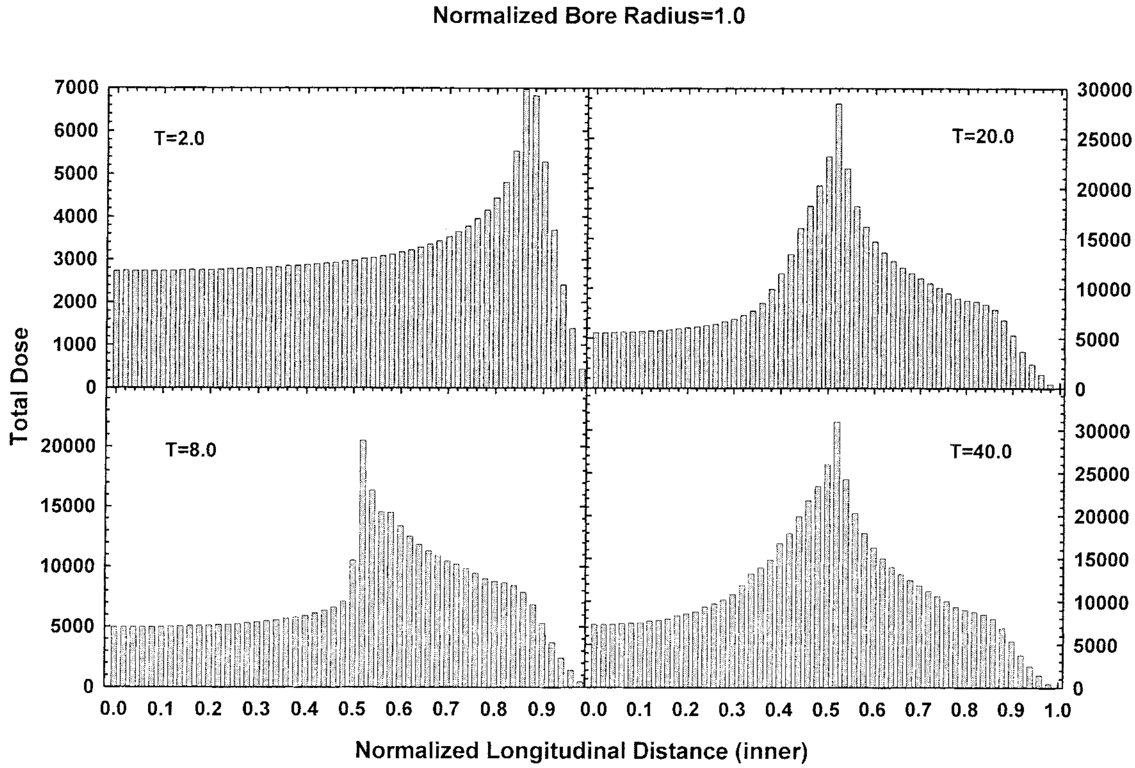

(a)

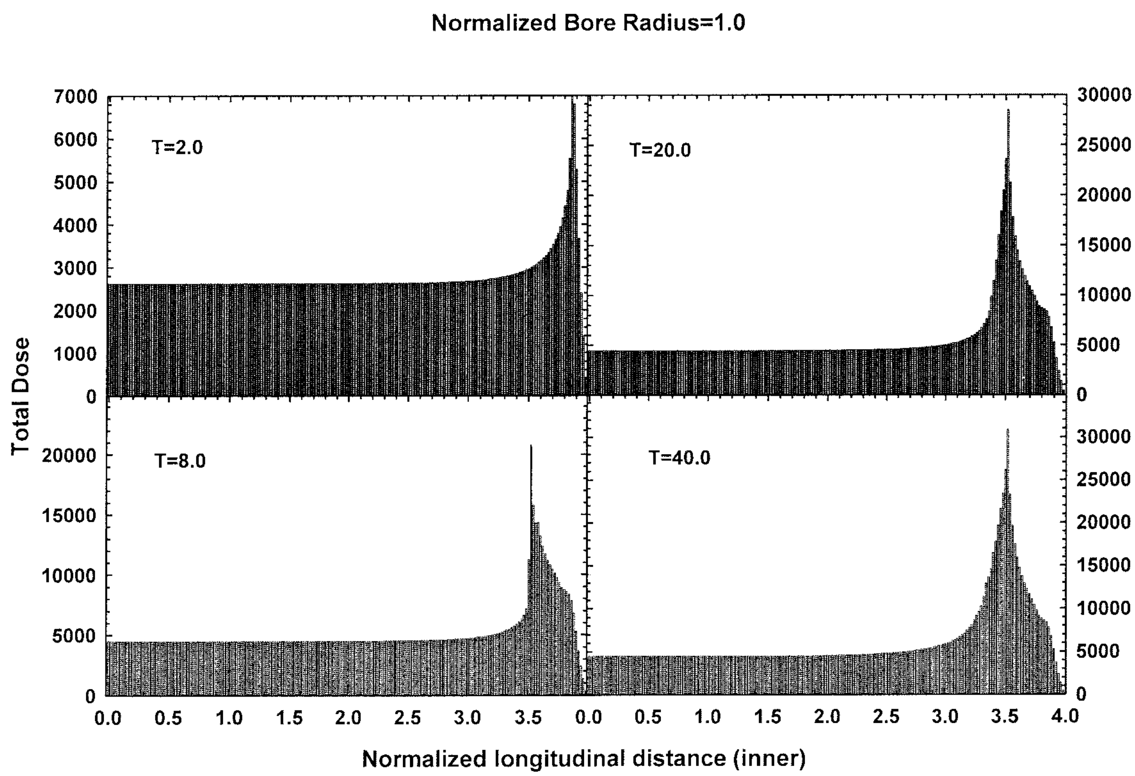

(b)

Fig. 4. Evolution of the total incident dose along the inner surface of the bore for (a) radius = 1D, half-length = 1D and (b) radius = 1D, half-length = 4D.

as depicted in Fig. 3(c) and (d). At $t = 40T_{pi}$, the inside of the tube is observed to be empty. The density oscillations observed along the longitudinal axis and above the top of the tube are due to the sheath edge lying along a row or column and jumping from grid lines to grid lines.

C. Total Dose

The local incident doses along the inner surface of the tube are displayed in Fig. 4. The two cases of bore radius equal to 1.0 are shown in Fig. 4(a) and (b). The other two cases of bore radius equal to 0.5 are exhibited in Fig. 4(c) and (d).

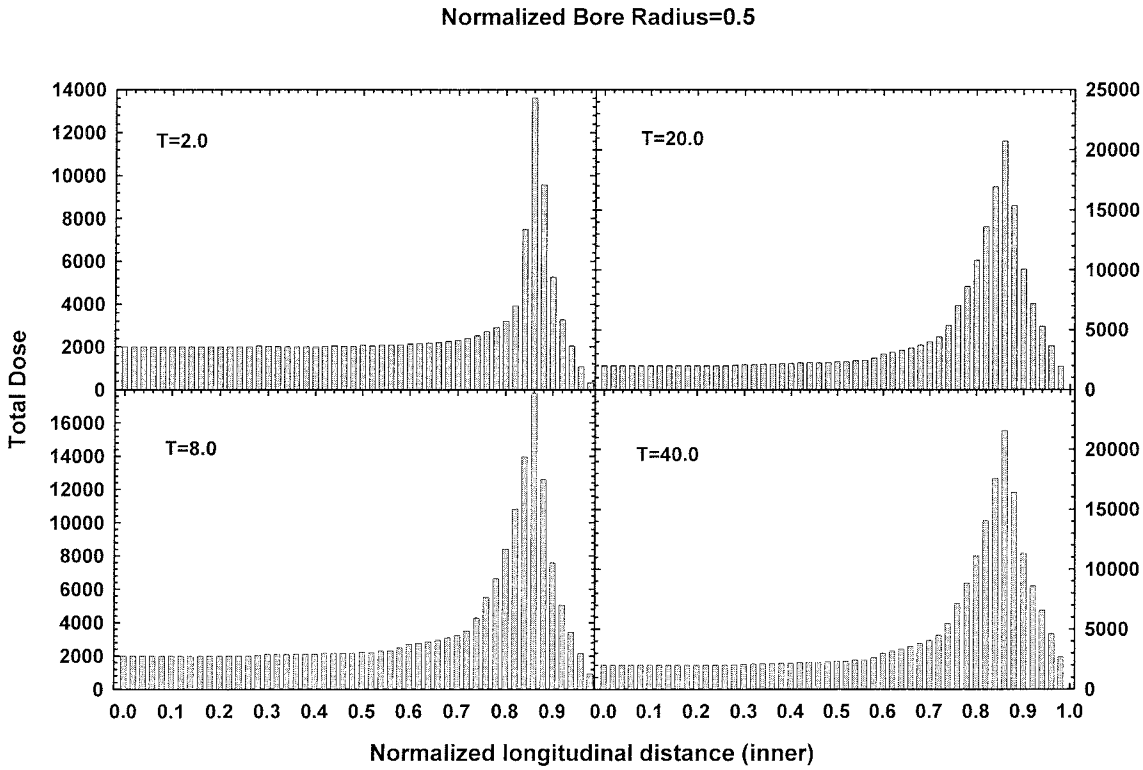

(c)

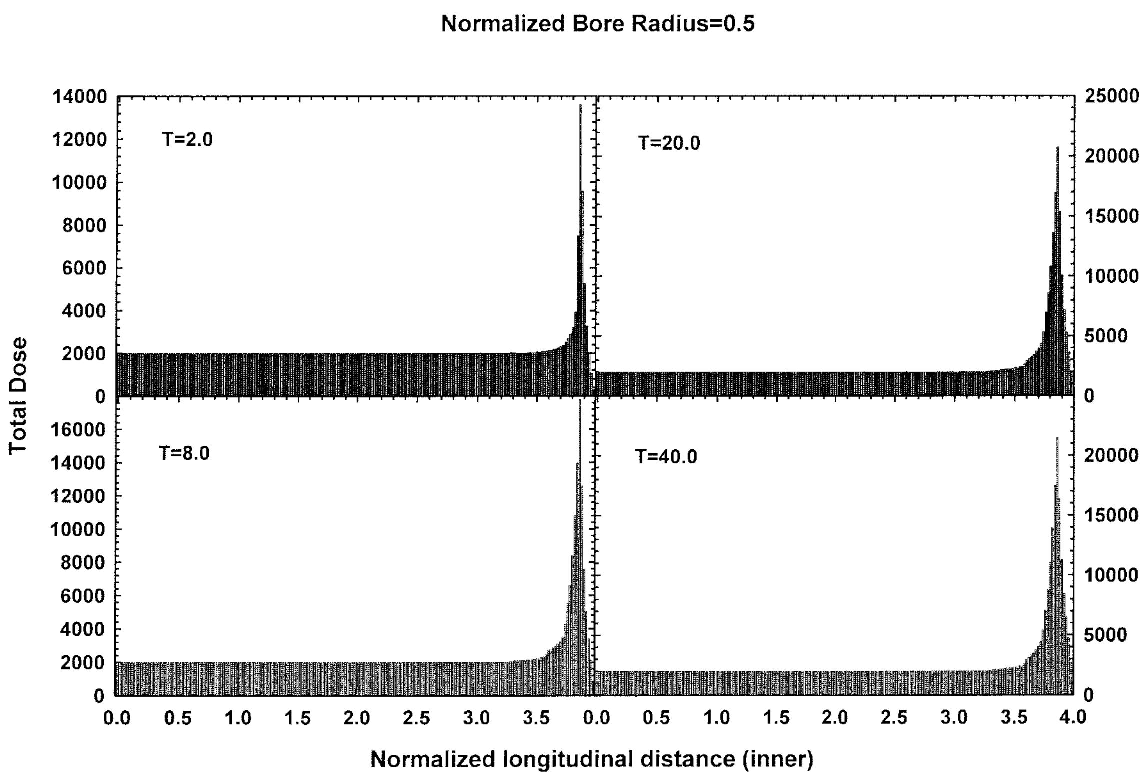

(d)

Fig. 4. *(Continued.)* Evolution of the total incident dose along the inner surface of the bore for (c) radius = 0.5D, half-length = 1D and (d) radius = 0.5D, half-length = 4D.

Initially, the inner surface of the bore is evenly implanted except a small peak at the top of the bore where the electric field is concentrated. After some time, the deeper region of the bore is not implanted. The total dose reaches 5000 as shown in Fig. 4(a) and (b) (bore radius = 1.0 D), but only 2000 as shown in Fig. 4(c) and (d) (bore radius = 0.5 D). Only a small region of the inner surface continues to get implanted at later time as illustrated by the instantaneous dose (D) and impact

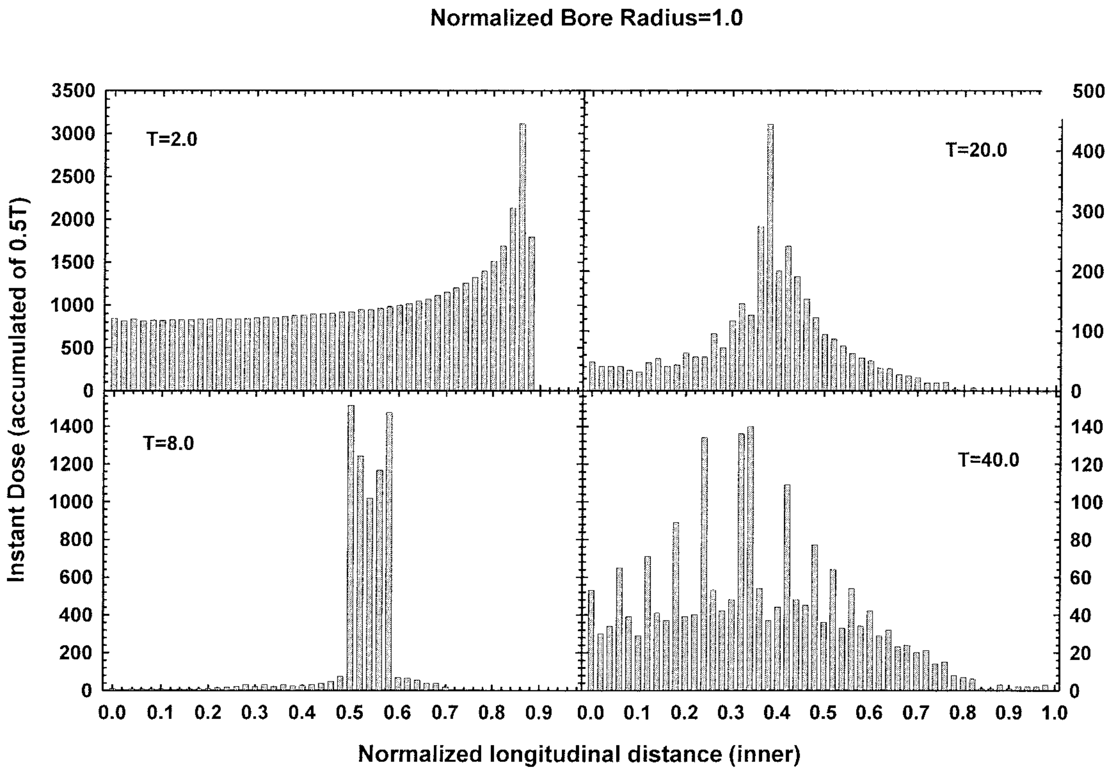

(a)

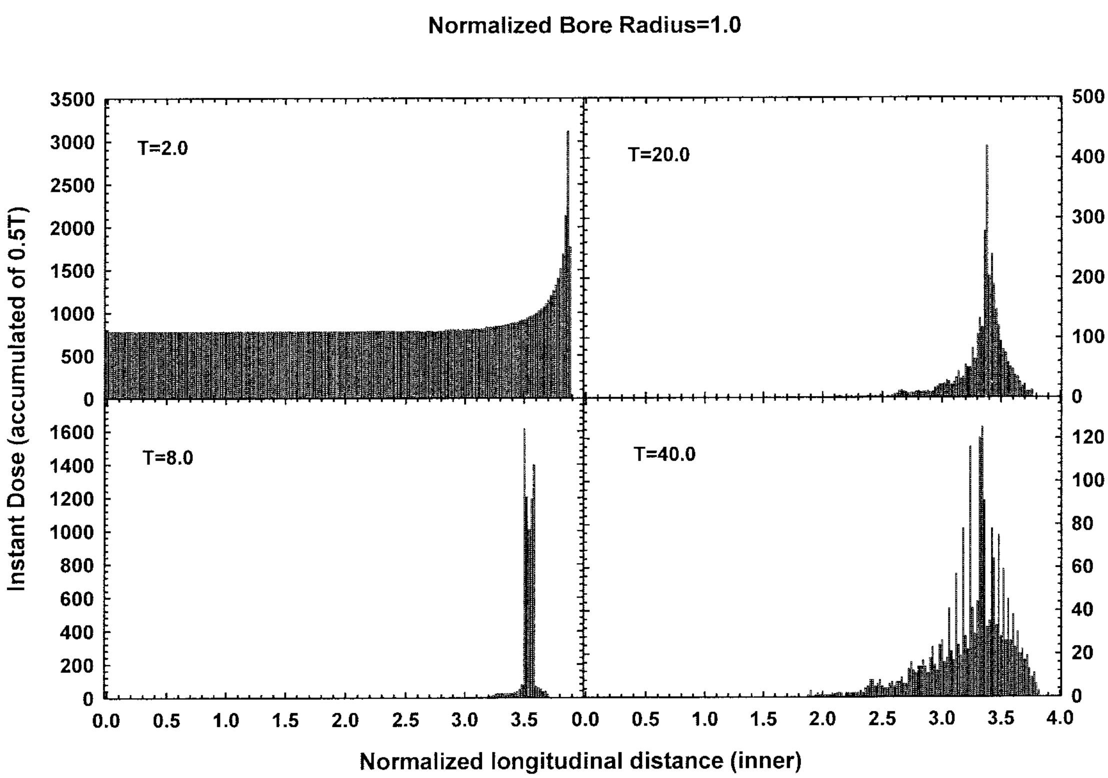

(b)

Fig. 5. Evolution of the instant dose (0.5T accumulation) along the inner surface of the bore for (a) radius = 1D, half-length = 1D and (b) radius = 1D, half-length = 4D.

angle (E). The total dose peaks at 0.5 D from the top of the bore for a bore radius of 1.0 D as shown in Fig. 4(a) and (b). When the bore radius is 0.5 D, the peak is located at 0.15 D from the top of the tube as shown in Fig. 4(c) and (d).

D. Instantaneous Dose

The instantaneous incident dose along the inner surface of the tube using an accumulation of $0.5T_{pi}$ is depicted in Fig. 5. When the bore radius is 1.0 at t is $2.0T_{pi}$, around 700 ions

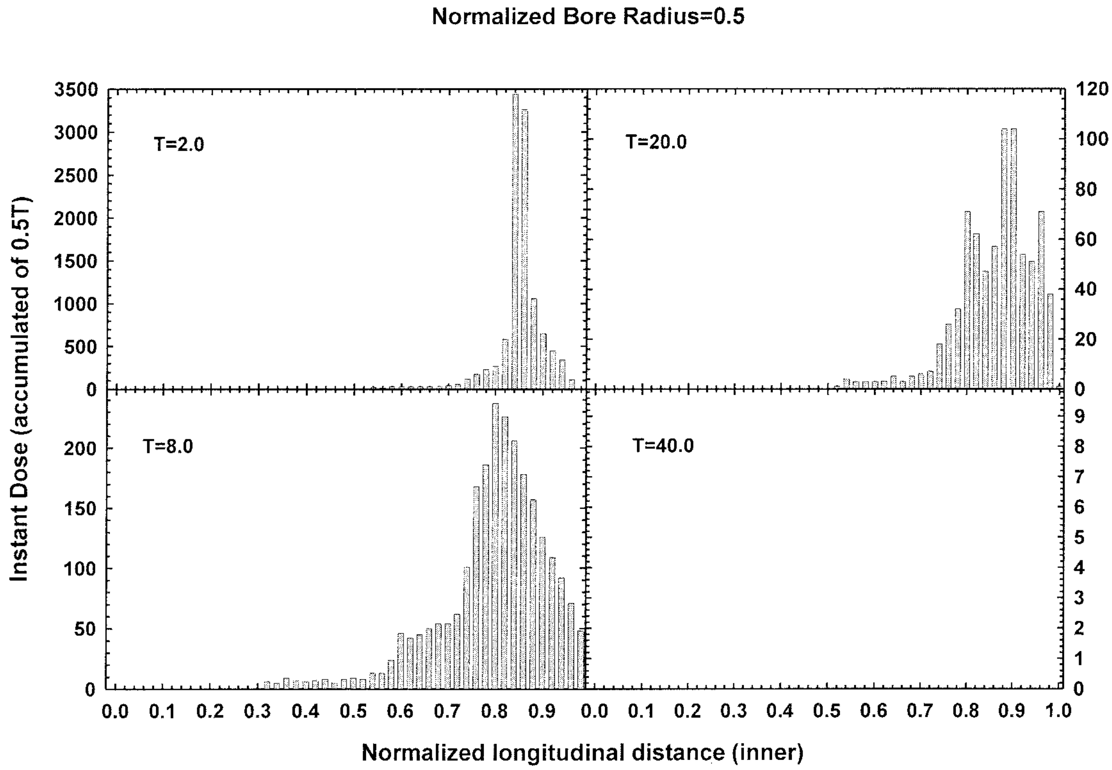

(c)

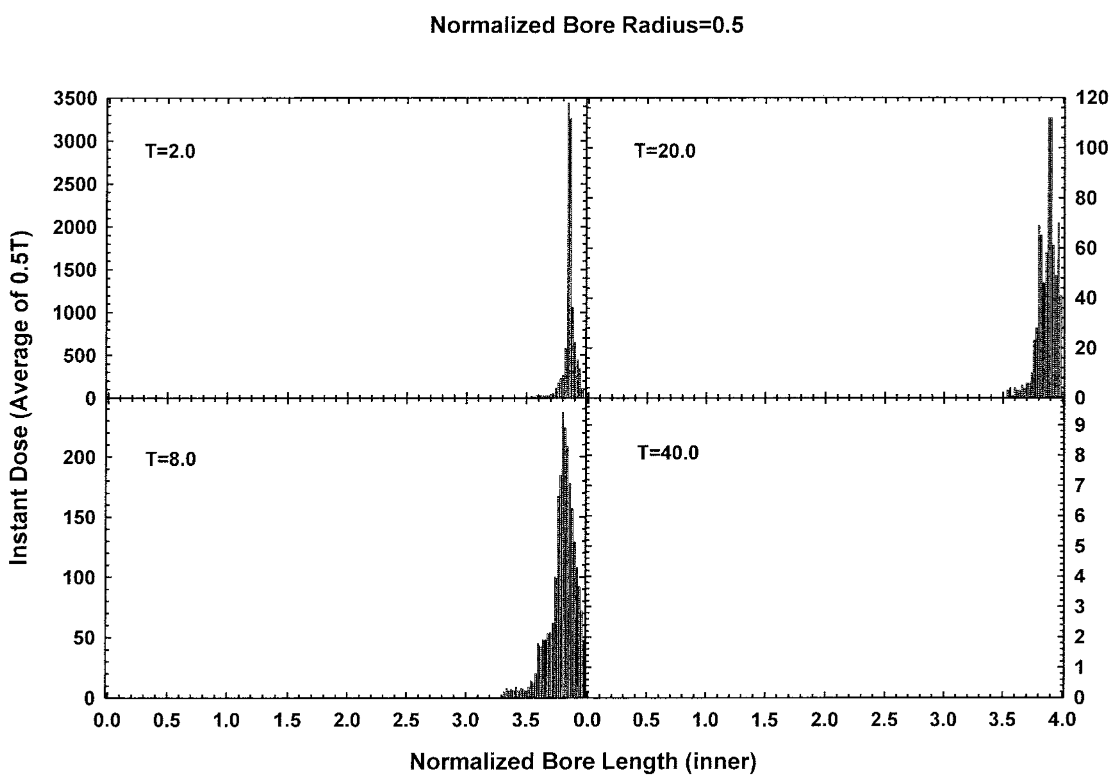

(d)

Fig. 5. *(Continued.)* Evolution of the instant dose (0.5T accumulation) along the inner surface of the bore for (c) radius = 0.5D, half-length = 1D and (d) radius = 0.5D, half-length = 4D.

(100 ions per cell) are implanted evenly along the inner surface except at the top of the bore as shown in Fig. 5(a) and (b). However, after the ions present initially inside the bore have been exhausted, outside ions with an impact angle less than 180 degree [see instant impacted angle (E)] are implanted into a small region 0.5 D from the top of the bore. No ions arrive

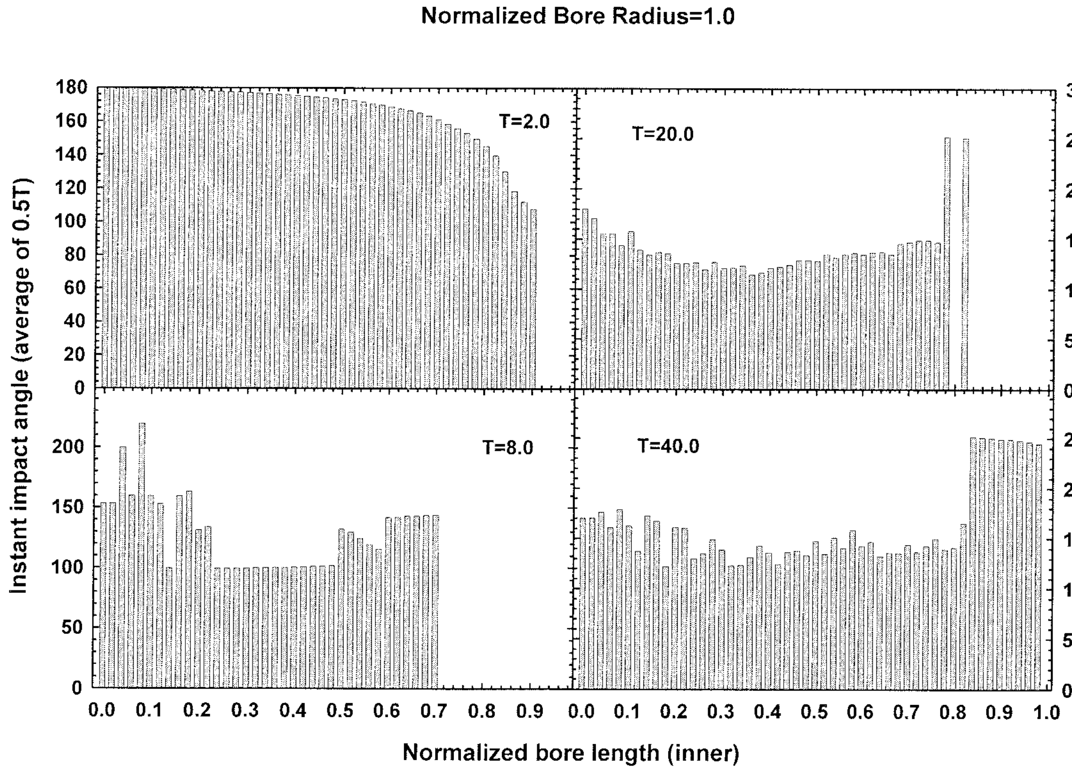

(a)

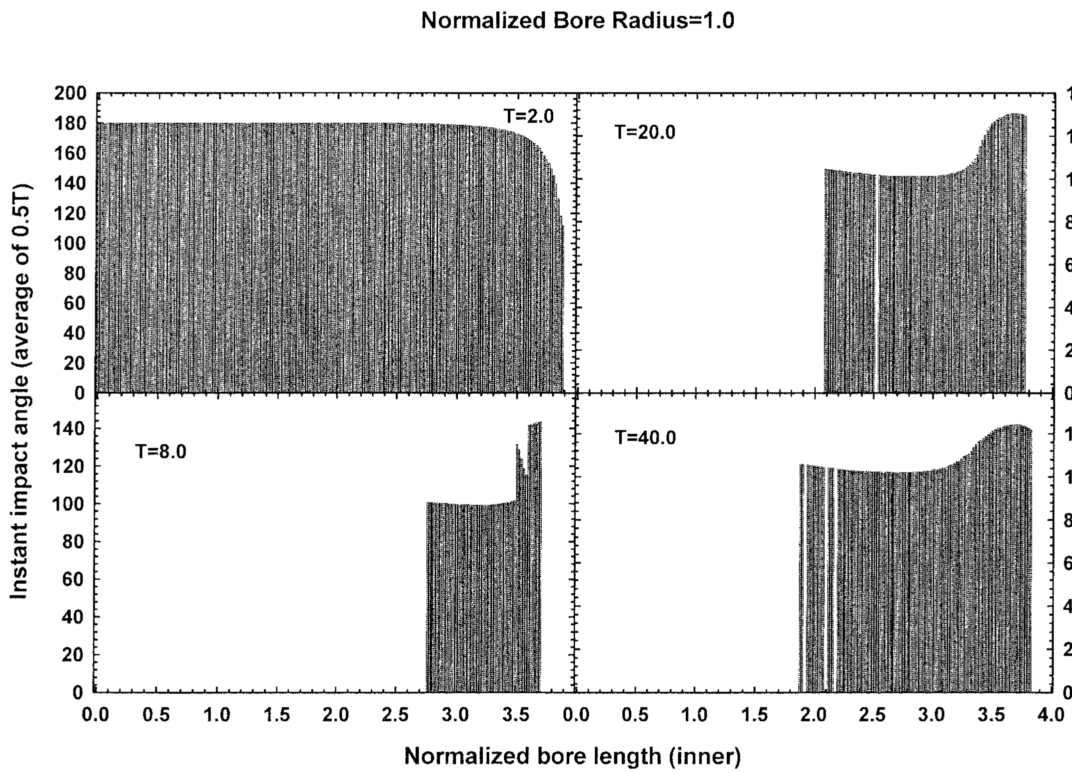

(b)

Fig. 6. Evolution of the instant impact angle (average of 0.5T) along the inner surface of the bore for (a) radius = 1D, half-length = 1D and (b) radius = 1D, half-length = 4D.

at the rest of the surface when the bore length (half) is longer than 1.0 D. Therefore, a peak of accumulated implanted dose is observed at this area exhibited in Fig. 4(a) and (b).

Fig. 5(c) and (d) depict the case of bore radius equal to 0.5 D. When the bore is narrower, the ions inside the bore are exhausted sooner and outside ions are implanted into an area

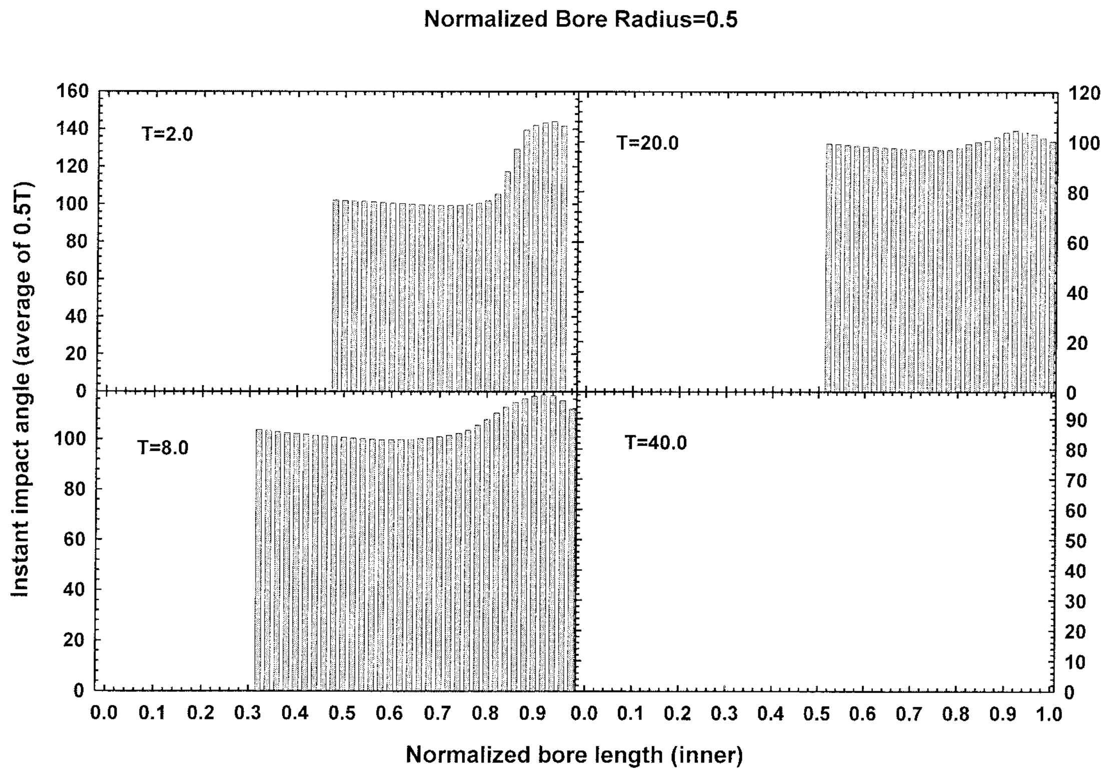

(c)

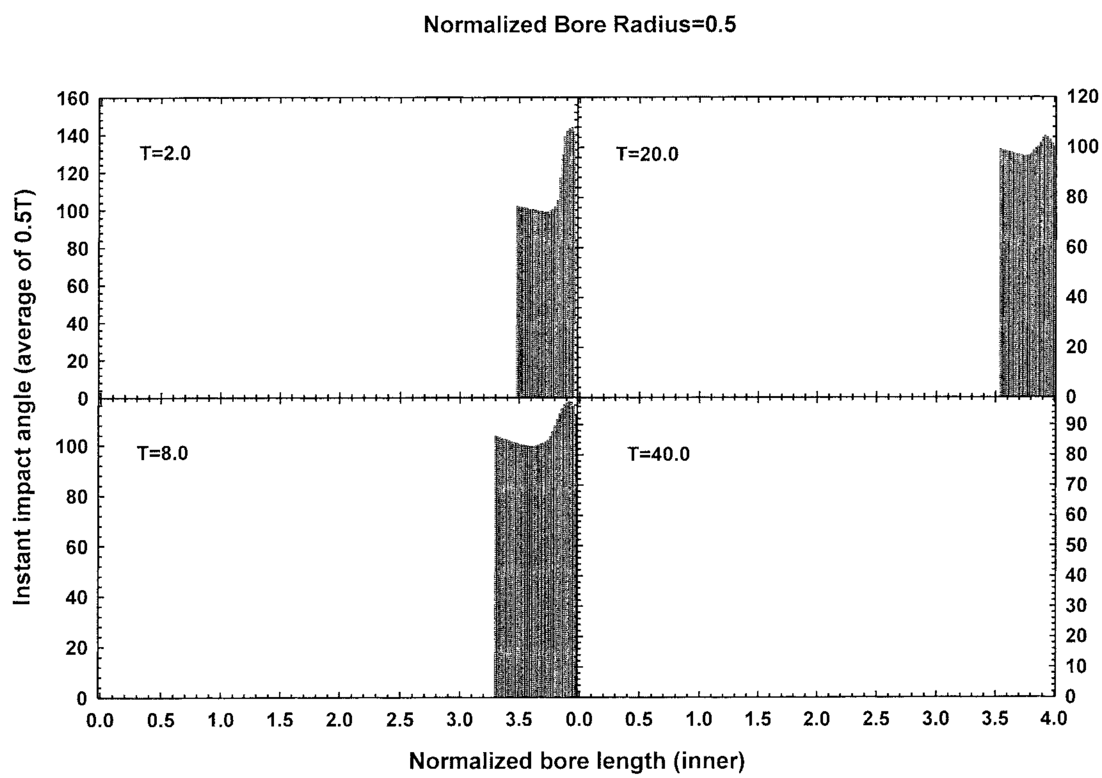

(d)

Fig. 6. *(Continued.)* Evolution of the instant impact angle (average of 0.5T) along the inner surface of the bore for (c) radius = 0.5D, half-length = 1D and (d) radius = 0.5D, half-length = 4D.

0.15 D from the top of the bore as shown in Fig. 5(c) and (d). In both cases, it can be observed that the ions implanted into the inner surface decrease with time. In fact, as shown in Fig. 5(c) and (d), no ions arrive at $t = 40T_{pi}$. Therefore, the total accrued dose into the inner surface of the bore will not increase anymore.

E. Impact Angle

The impact angle of the ions along the inner surface of the bore using an average of $0.5T_{pi}$ is depicted in Fig. 6. The impact angle θ is defined in Fig. 1. If there is no ion impact, the impact angle will be set to zero. As shown in Fig. 6(a) and (b) with bore radius of 1.0 D and t equal to $2.0T_{pi}$, most of the implanted ions incident at a normal angle except near the top region. Some of the ions come from outside of the tube and can pass through the midplane of the bore to be implanted into the other side. However, the chance becomes smaller if the tube length is larger or narrower. As displayed in Fig. 6(a), at a later time, the impact angle can be larger than 180°. These ions must come from the other side of the bore with velocity pointing upward and at $t = 40T_{pi}$, these ions arrive at the top of the bore. Fig. 6(b)–(d) does not reveal any impact angle greater than 180° and no ions have passed through the midplane.

IV. Conclusion

For the practical case when the bore length is finite, our results show that after all the ions present initially in the bore have been exhausted, outside ions are influenced by the auxiliary electrode and implanted into a small area near the top of the bore. A local region with a maximum total dose thus results. When the bore radius is 1.0/0.5 D, the peak is located at 0.5/0.15 D from the top of the bore. If the bore is short, some of the ions can pass through the midplane of the bore and land on the other side. We have observed that some of the ions can indeed pass through the midplane of the bore and get implanted into the top of bore. The impact angle of these ions points upwards. However, as the bore gets longer, the chance of these outside ions passing through diminishes. They will thus not add to the accrued dose in the deeper region of the bore. Provided that the bore is long enough, we can conceptually divide the inner bore surface into a middle region and an end region covering the rest of the bore. According to our results, the boundary between the "middle" and "end" regions can be demarcated at 1.0/0.5 D from the top of the bore for a bore radius of 1.0/0.5 D. Implantation into the middle region can thus be simplified and simulated by a 1-D model [8]. For example, we can use the 1-D normalized PIC equations

$$\frac{\partial^2\Psi}{\partial\rho^2}+\frac{1}{\rho}\,\frac{\partial\Psi}{\partial\rho}=N_e-N_I \tag{4a}$$

$$\Delta\rho=\frac{V_\rho^a\Delta T}{\sqrt{2}}+\frac{1}{8}\,\frac{\partial\Psi}{\partial\rho}\,(\Delta T)^2 \tag{4b}$$

$$\Delta V_\rho=\frac{1}{\sqrt{8}}\,\frac{\partial\Psi}{\partial\rho}\,\Delta T. \tag{4c}$$

The simulation results are in good agreement with our experimental results reported elsewhere.

References

[1] T. E. Sheridan, "Ion-matrix sheath in a cylindrical bore," *J. Appl. Phys.*, vol. 74, no. 8, pp. 4903–4906, 1993.

[2] M. Sun, S. Yang, and B. Li, "New method of tubular materials inner surface modification by plasma source ion implantation," *J. Vac. Sci. Technol. A*, vol. 14, no. 2, pp. 367–369, 1996.

[3] M. Sun and S. Yang, "Measurements of spatial and temporal sheath evolution inside tubular material for inner surface ion implantation," *J. Vac. Sci. Technol. A*, vol. 14, no. 6, pp. 3071–3074, 1996.

[4] T. E. Sheridan, "Sheath expansion into a large bore," *J. Appl. Phys.*, vol. 80, no. 1, pp. 66–69, 1996.

[5] ———, "Pulsed sheath dynamics in a small cylindrical bore," *Phys. Plasma*, vol. 1, pp. 3485–3489, 1994.

[6] ———, "Analytic theory of sheath expansion into a cylindrical bore," *Phys. Plasma*, vol. 3, no. 9, pp. 3507–3512, 1996.

[7] X. C. Zeng, B. Y. Tang, and P. K. Chu, "Improving the plasma immersion ion implantation impact energy inside a cylindrical bore by using an auxiliary electrode," *Appl. Phys. Lett.*, vol. 69, no. 25, pp. 3815–3817, 1996.

[8] X. C. Zeng, T. K. Kwok, A. G. Liu, P. K. Chu, B. Y. Tang, and T. E. Sheridan, "Effects of the auxiliary electrode radius during plasma immersion ion implantation of a small cylindrical bore," *Appl. Phys. Lett.*, vol. 71, no. 8, pp. 1035–1037, 1997.

[9] T. E. Sheridan, T. K. Kwok, and P. K. Chu, "Kinetic model for plasma-based ion implantation of a short, cylindrical tube with auxiliary electrode," *Appl. Phys. Lett.*, vol. 72, no. 15, pp. 1826–1828, 1998.

[10] A. G. Liu, X. F. Wang, B. Y. Tang, and P. K. Chu, "Dose and energy uniformity over inner surface in plasma immersion ion implantation," *J. Appl. Phys.*, vol. 84, no. 4, pp. 1859–1862, 1998.

[11] T.-K. Kwok, Paul K. Chu, and C. Chan, "Ion dose uniformity for planar sample plasma immersion ion implantation," *IEEE Trans. Plasma Sci.*, vol. 26, pp. 1669–1679, Dec. 1998.

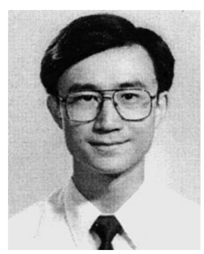

Dixon Tat-Kun Kwok received the B.Sc. degree in physics in 1988 and the Ph.D. degree in solid-state physics in 1993 from King's College London, University of London, U.K.

From April 1994 to March 1995 he served as a Postdoctoral Fellow at the Surface Physics Lab, Fudan University, Shanghai, China. From April 1995 to June 1996 he was a Research Associate in the Physics Department, Hong Kong University of Science and Technology, Hong Kong. Currently, he is a Research Fellow in the Department of Physics and Material Science, City University of Hong Kong. He has published papers on topics related to photoluminescence and photo absorption of point defects in silicon, reflectance difference spectroscopy, and numerical simulation of plasma immersion ion implantation.

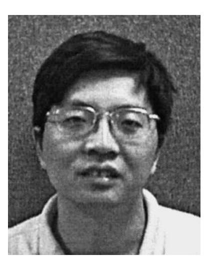

Xuchu Zeng (M'97) was born in Sichuan, China, on February 12, 1964. He received the B.S. degree in electrical engineering from Xian JiaoTong University, China, in 1985 and the M.S. degree in plasma physics from Southwestern Institute of Physics, China, in 1991. He is currently working towards the Ph.D. degree at the City University of Hong Kong.

He was appointed Assistant Engineer, Engineer, and Senior Engineer in 1986, 1992, and 1994, respectively, at the Southwestern Institute of Physics. From June 1995 to June 1997, he was a research staff member in the Plasma Laboratory at the City University of Hong Kong. His research interests include plasma immersion ion implantation equipment design as well as applications.

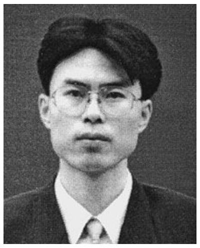

Qingchuan Chen was born in Zhejiang, China, on March 24, 1970. He received the B.S. degree in computer-aided machine design and manufacturing from Xian Jiaotong University, China, in 1992.

He joined the Southwestern Institute of Physics, China, in 1992 and was appointed Assistant Engineer and Engineer in 1993 and 1997, respectively. He was also the Vice-Director of the Ion Beam Development and Application Center of the Southwestern Institute of Physics. He is currently working as a Research Assistant in thePlasma Laboratory of the City University of Hong Kong. His research interests include plasma immersion ion implantation as well as other ion beam implantation technologies and hardware.

Paul K. Chu (M'97) received the B.S. degree in mathematics from The Ohio State University, Columbus, in 1977 and the M.S. and Ph.D. degrees in chemistry from Cornell University, Ithaca, NY, in 1979 and 1982, respectively.

He joined Charles Evans & Associates in California in 1982 and assumed various technical and managerial positions. He founded Evans Asia in early 1990 and later joined the City University of Hong Kong as a visiting faculty member. He is currently a Professor at the City University of Hong Kong, Fudan University, and Peking University in China. His research activities include plasma processing technology and materials characterization.

Dr. Chu is a member of the American Chemical Society, the Materials Research Society, and the Böhmische Physical Society and a Fellow of the Hong Kong Institution of Engineers.

Terrence E. Sheridan received the B.A. degree in physics from Hiram College, Hiram, OH, in 1983 and the Ph.D. degree in plasma physics from Dartmouth College, Hanover, NH, in 1987.

He held postdoctoral appointments at the University of Iowa, Iowa City, and West Virginia University, Morgantown, and has taught at Glenville State College, Glenville, WV. Currently, he holds a research fellowship in the Space Plasma and Plasma Processing Group at the Australian National University, Canberra, Australia. His research interests include experimental characterization and simulation of sputtering magnetron discharges, dusty plasmas, plasma sheath dynamics, particularly the interior problem and two-dimensional targets, and the theory and modeling of ion-acoustic solitons. He has authored more than 50 publications.